metals

MDPI

Article

Transparent Silver Coatings with Copper Addition for Improved Conductivity by Combined DCMS and HiPIMS Process

Catalin Vitelaru [1], Anca C. Parau [1], Mihaela Dinu [1], Iulian Pana [1,*], Lidia R. Constantin [1], Arcadie Sobetkii [2] and Iulian Iordache [3]

[1] National Institute of Research and Development for Optoelectronics-INOE 2000, 409 Atomiștilor Street, 077125 Magurele, Romania; catalin.vitelaru@inoe.ro (C.V.); anca.parau@inoe.ro (A.C.P.); mihaela.dinu@inoe.ro (M.D.); lidia.constantin@inoe.ro (L.R.C.)
[2] SC MGM Star Construct SRL, 7 Pancota Street, 022773 Bucharest, Romania; sobetkii@yahoo.com
[3] National Institute for Research and Development in Electrical Engineering ICPE-CA Bucharest, 313 Splaiul Unirii, 030138 Bucharest, Romania; iordache@icpe-ca.ro
* Correspondence: iulian.pana@inoe.ro; Tel.: +40-21-457-57-59

Abstract: The demand for transparent conductive coatings has increased over recent years, leading to the development of various technical solutions. One of the approaches is to use metallic coatings very close to their coalescence thickness, so that a good compromise between transparency and conductivity is obtained. In this contribution, a combination of two elements with high potential in this field is used, namely silver and copper. The continuity of silver films on a dielectric transparent substrate is significantly improved by the addition of a copper seed layer that promotes the formation of a continuous layer at smaller effective thicknesses. Two distinct deposition processes are used for the deposition of the two materials, namely HiPIMS (High Power Impulse magnetron sputtering) for copper and DC sputtering for silver. The use of HiPIMS enables a better control of the structure and quantity of deposited material, allowing us to deposit a very small amount of material. The mono-element coatings are characterized from the optical and electrical point of view, and then mixed to form a structure with better transparency, up to 80% in the visible spectrum, good electrical properties, resistivity of ~2 × 10^{-5} (Ω × cm), and significantly lower surface roughness, down to 0.2 nm.

Keywords: HiPIMS; thin films; silver; transparent conductive; magnetron sputtering

check for updates

Citation: Vitelaru, C.; Parau, A.C.; Dinu, M.; Pana, I.; Constantin, L.R.; Sobetkii, A.; Iordache, I. Transparent Silver Coatings with Copper Addition for Improved Conductivity by Combined DCMS and HiPIMS Process. *Metals* **2022**, *12*, 1264. https://doi.org/10.3390/met12081264

Academic Editor: Qingping Cao

Received: 31 May 2022
Accepted: 25 July 2022
Published: 27 July 2022

Publisher's Note: MDPI stays neutral with regard to jurisdictional claims in published maps and institutional affiliations.

Copyright: © 2022 by the authors. Licensee MDPI, Basel, Switzerland. This article is an open access article distributed under the terms and conditions of the Creative Commons Attribution (CC BY) license (https://creativecommons.org/licenses/by/4.0/).

1. Introduction

The deposition of thin metal films on insulating substrates or layers is of great interest, with applications in the field of nanoelectronics [1,2], energy saving and energy conversion [3–5], and electromagnetic interference shielding [6]. The use of such thin films obtained from the vapor phase is limited by the uncontrolled three-dimensional morphology characteristic on the initial stages of film growing [7,8]. The ability of the forming layer to uniformly wet the surface and form a continuous two-dimensional film becomes of great importance. The minimum thickness achievable becomes of even greater importance for the applications where the transparency of the film is required, such as low-e coatings for windows [9–11], electromagnetic shielding [6] and more generally transparent conductive layers [12,13].

There are different solutions to reduce the minimum thickness necessary for obtaining a continuous layer. Among those, the use of a small addition of O_2 or N_2 to the Ar gas was proven to be beneficial for the promotion of 2D growth of Ag films [14–16]. The presence of N_2 or O_2 in the sputtering gas atmosphere appears to decrease the rates of island coalescence completion, with a minor effect on the conductivity of the coating due to the incorporation of O or N [7]. Another solution is to use various doping elements to change the ability of forming a metallic layer to wet the surface. Al, Cu, Nb, Ti, etc., are

the most common elements that are frequently used for this purpose [17,18], leading to a reduction of the surface roughness and the minimum thickness achieved. The use of a two-step process consisting of the deposition of an initial seed layer before the actual thin film was also successfully employed [19]. It was already shown that the addition of Cu in the initial stages of Ag deposition leads to a smoother surface and allows for smaller thicknesses of the continuous layer [7]. Copper was introduced in the first stages of growth, accounting for equivalent thicknesses of only ~2 nm. The choice of Cu as seed layer or wetting agent for Ag films is related to the tendency to promote the 3D growth less initially [20], and to the fact that the two metals are immiscible at room temperature [21,22], making the influence on the chemistry of the metal negligible. The effect of copper as a wetting agent for the growth of Ag films on SiO_2 substrates was recently detailed in Ref. [7], emphasizing the positive effects of Cu addition on decreasing both the roughness and the resistivity of the films. Moreover, it is concluded that the precise timing of the Cu arrival only at the initial stages of the process is of great importance for obtaining the wetting effect without compromising the electrical properties of the Ag layer.

Among the sputtering techniques, HiPIMS [23] stands as a versatile tool to obtain controllable properties, through the fine tuning of the deposition flux and energy to the substrate [24,25]. The pulsed nature of the process allows the use of the number of pulses as an element of fine adjustment of the quantity of deposited atoms. The deposition rates can be so low that hundreds of even thousands of pulses are necessary to obtain the equivalent of 1 atom thick layer.

In the present study, we demonstrate the use of HiPIMS deposited Cu as a wetting agent for the deposition of continuous and conductive Ag layers on transparent glass substrates. The deposition is performed in an industrial deposition chamber, allowing us to obtain uniform coatings on a 10×10 cm^2 square surface. The optical and electrical properties of Cu and Ag nanometric monolayers are assessed, with the purpose of obtaining the optimum combination of a Cu-Ag layer with minimum thickness, high transmission in the visible range and low resistivity.

2. Materials and Methods

The experimental setup consisted of Z-550-S (Leybold-Heraeus, Cologne, Germany) vacuum chamber 550 mm in diameter and 100 mm height. Two cathodes of Ag and Cu with a diameter of 6 inches are placed in the upper side of the deposition chamber, whereas the soda lime glass substrates are placed on a rotatable substrate holder at a distance of 60 mm from the magnetron targets, on the bottom side of the chamber. The base pressure in the discharge chamber is 2×10^{-5} mbar, and the working pressure is set at 10^{-2} mbar of Ar. The Cu target is powered by a HiPIMS power supply (Ionautics, Linköping, Sweden), whereas the Ag target is powered by DC powers supply SSV-3,5KW (Leybold-Heraeus, Cologne, Germany). The DC power input on the Ag target was varied between 100 W and 250 W, whereas the HIPIMS power on the Cu target was varied between 150 W and 750 W, to obtain different thicknesses of the coatings.

The use of a HiPIMS power supply for the Cu deposition allows us to obtain a fine control over the amount of deposited Cu through the variation of the frequency of the pulses. In order to maintain the same characteristics of the sputtered flux, the pulse width and amplitude were kept constant, whereas the frequency of the pulses was changed to reach the desired average power. The pulse voltage and current time traces are represented in Figure 1, indicating that pulse shape, amplitude and power were kept constant for all HiPIMS power settings.

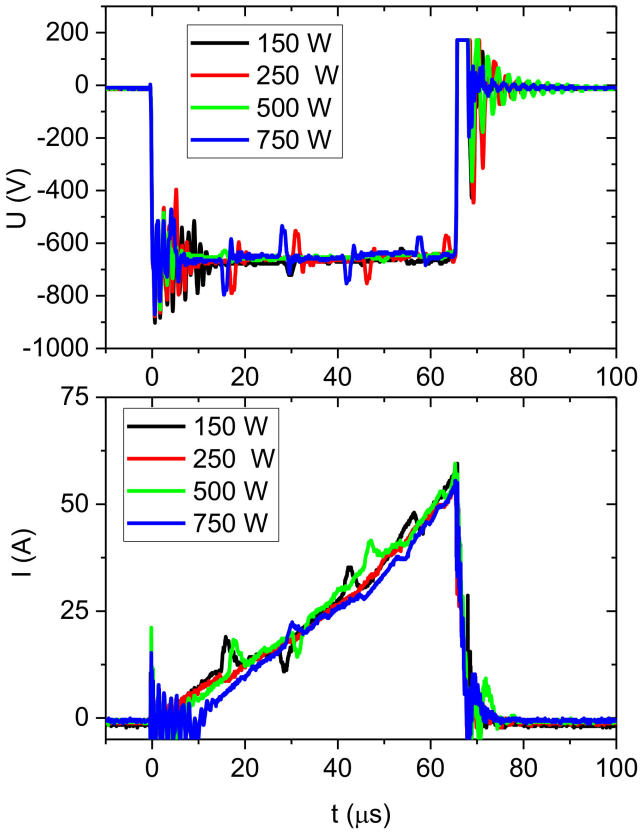


Figure 1. Electrical characteristic of the pulses used for deposition of Copper in HiPIMS mode at different average power and same peak current of ~60 A.

The deposition process is adapted to an industrial-sized deposition chamber, where the combination of power input and target sizes gives deposition rates higher than needed for this application. Therefore, one of the main characteristics of the deposition process is its very short duration, of only 10 s, giving total thicknesses in the 5–20 nm range. This total duration is obtained by passing the substrates in front of the targets with an angular velocity that gives one complete rotation for every 10 s. In this way, it is possible to obtain both the monolayer structures and the bilayer structures that contain successive layers of Cu and Ag, respectively. It should be noted that the minimum power input used for these processes is found at the bottom limit of the power supply, meaning that further decrease of the power would lead to unstable discharge conditions in the given sputtering geometry and gas pressure range. The abbreviated sample names are presented in Table 1, comprising the type of power supply and the power input. The deposition time is set to 10 s for all the samples that will be analyzed in the following.

Table 1. Codification of samples depending on type of power supply and power applied to the cathodes.

Sample Name	Power Supply Type	Power (W)	Deposition Time
AgDC100	DC	100	10 s
AgDC150	DC	150	10 s
AgDC200	DC	200	10 s
AgDC250	DC	250	10 s
CuHiP150	HiPIMS	150	10 s
CuHiP250	HiPIMS	250	10 s
CuHiP500	HiPIMS	500	10 s
CuHiP750	HiPIMS	750	10 s

Film thickness was determined by surface profilometry measurements with Veeco NT1100 system (Veeco Instruments, Plainview, NY, USA) operating in a vertical scanning interferometry (VSI) mode. Thin films were chemical acid etched to obtain a step profile that allows determining the film thickness. The 10× magnification lens and a 0.5× field of view (FOV) lens were used on 191 µm × 255 µm surface. Optical characterization of the samples was performed by UV-Vis-NIR spectrophotometry using a Jasco V-670 spectrophotometer (Jasco, Tokyo, Japan) with an attached ARSN 733 unit. The transmittance and reflectance of the deposited coatings were recorded in the same spot at near-normal incidence (5°). The absolute reflectance measurement accuracy provided by the supplier is ±1.5% at 6° angle of incidence. The absorbance spectra was calculated by using the following formula A = 100 – T (%) − R (%). The XRR measurements were performed using SmartLab diffractometer (RIGAKU, Tokyo, Japan) equipped with Cu rotating anode (9 kW) and vertical goniometer with 5 axes. The measurements were performed on a 2θ range of 0.3–3°, with a speed of 0.16°/min and a step size of 0.004°. Surface morphology was investigated by using AFM/STM Microscopy System (INNOVA VEECO, Berlin, Germany), working in taping mode. Morphological characterization was performed with FESEM-FIB Scanning Electron Microscope (Carl Zeiss, Jena, Germany) equipped with an energy dispersive X-ray detector (Oxford Instruments, Oxford, UK). The images were recorded at 100 k× magnification. Electrical characterization was made using a Cascade C4S-64/50 with four-point probes placed at equal distances using a constant current source, Keithley 2400/2400-C Source Meter (200 V, 1 A, 20 W), for measuring electrical resistivity and surface resistance. Measurements were performed according to the method described in ASTM F 84–99 [26].

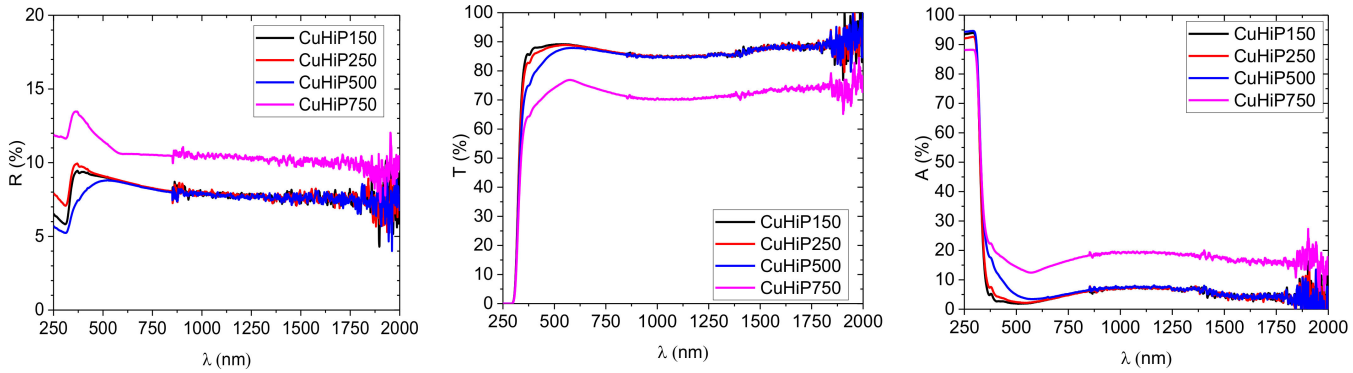
3. Results and Discussion

The results and discussion's part is divided in two sections, the first one referring to the monolayer's characterization and the second one to the bilayer structure consisting of one Cu interlayer and one Ag layer on top of it.

3.1. Optical and Electrical Properties of Cu and Ag Monolayers

The Cu layers were deposited using HiPIMS mode, with variable average power ranging from 150 to 750 W. The repetition frequency of the pulse was tuned correspondingly so that the peak current shape and amplitude remains constant in this interval, as described in the Materials and Methods section. Further decrease of the power below 150 W leads to the decrease of the peak current, down to 45 A. The main purpose was to identify the coalescence limit and then to define the deposition conditions that ensure the presence of a discontinuous layer.

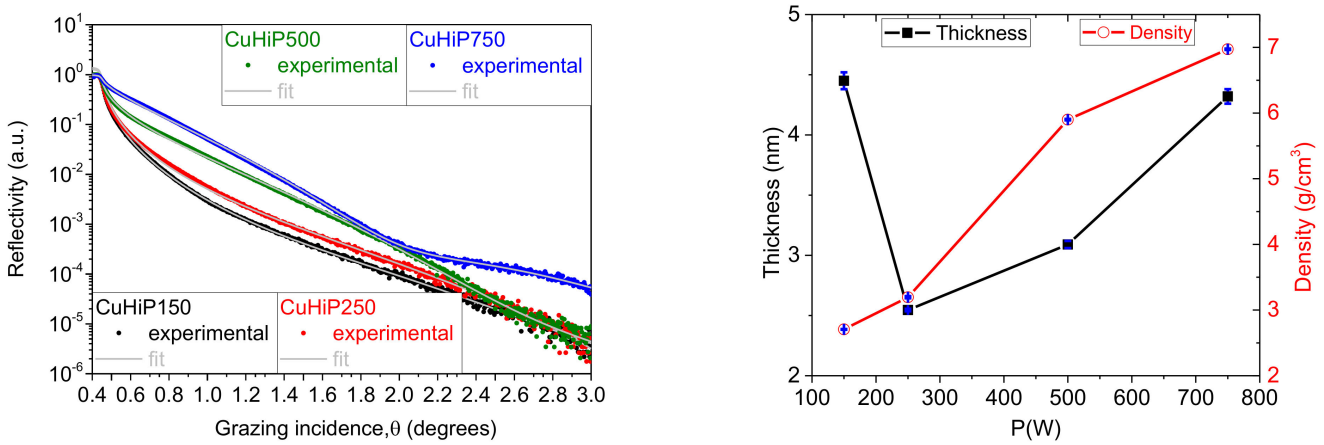
The optical properties of individual layers of Cu and Ag, respectively, were investigated by UV-Vis-NIR spectrophotometry, the curves registered between 250–2000 nm being presented in Figure 2. The high transparency and small reflection of the samples obtained at equivalent power of 150 and 250 W indicate that they are below the limit of coalescence. The sample obtained at 500 W reveals an increase of absorption in the 300 to 500 nm interval, indicating the presence of surface plasmon resonance due to the formation of nanometric clusters on the surface [27]. A more detailed study on the application of Mie theory applied to determine the optical properties of such films was described in Ref. [28]. More generally speaking, the increase of absorption it is a clear mark that these conditions are found at the limit of percolation [29]. One should note that the measurements were performed after air exposure of the samples, so oxidation of the very thin layer is expected. The samples obtained at 750 W equivalent power have a pronounced decrease of transparency and increase of both reflectivity and absorbance. This indicates that a continuous layer starts to form, and a further increase of power density would lead to a continuous metallic copper film.



(**a**) (**b**) (**c**)

Figure 2. Spectrophotometric curves, (**a**) reflectivity, (**b**) transmittance and (**c**) absorbance of Cu thin films deposited at different average HiPIMS power and a peak current of ~60 A.

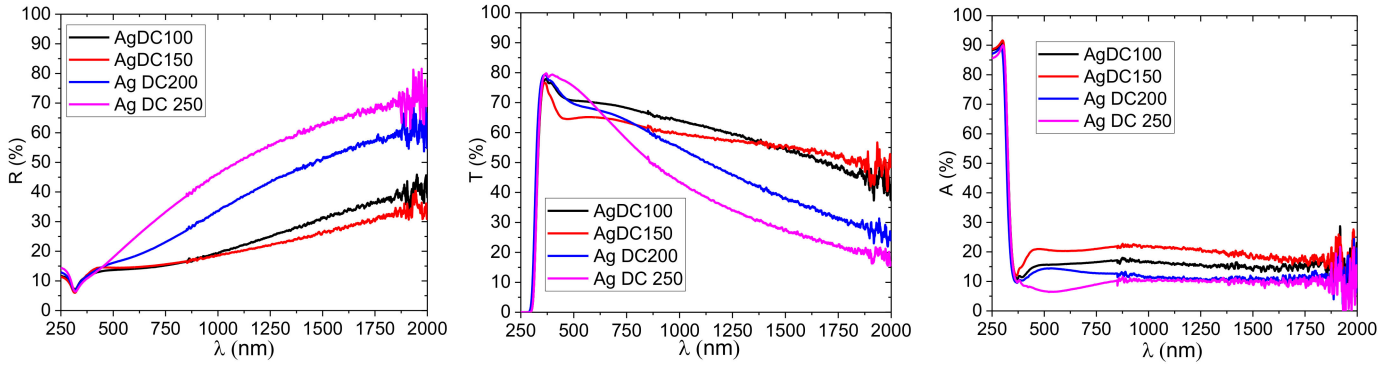
From the spectrometric data, we find that the best suited power setting for obtaining a discontinuous Cu layer is in the range of 150 to 250 W. To confirm this, XRR measurements were performed on all samples. The XRR spectra fitted with Rigaku GlobalFit software (based on Parallel Tempering algorithm, version 2.0.6.0, Tokyo, Japan) are represented in Figure 3a. Due to the discontinuous nature of the formed layer (with periodic voids arrangement) no visible interference induced oscillations were observed when lower sputtering power was applied. According to Buttard et al., the radiation interacts with a porous layer similar with the substrate, causing a strong decrease in reflected intensity [30]. Additionally, as it was reported in the literature, there is a high probability in obtaining featureless XRR patterns (with no fringe appearance) when nanometric monolayers based on islands formation are analyzed [31]. Extremely weak evidence of interference fringes can be observed when higher sputtering power was applied (750 W), result ascribed to a more continuous layer, characterized by less porosity present in this stage. The decay of reflectivity over the measured grazing-incident angle range further reveals the correlation between roughness and deposition conditions. There is an increasing tendency of surface roughness, starting from 0.69 nm (for CuHIP150 sample) up to 0.85 nm (for CuHIP500). By increasing the power at 750 W, the overall roughness decreases (0.58 nm) as the coalescence stage of neighboring clusters takes place. Indeed, during film formation, there is a tendency of reducing the surface area of the substrate by initially formed clusters [32]. However, the roughness value at these initial growth stages may be influenced by various factors influencing coverage area and the width and height profiles of cluster configurations [33]. The thickness and density evaluated from these spectra are represented in Figure 3b, indicating an almost linear increase of the density with increasing average power. The density at low power is significantly lower than bulk density of 8.96 g/cm^3, thus confirming the fact that the film is not continuous. The film thickness is in the interval from 2.5 to 5 nm, but this should be regarded as an averaged thickness of the individual islands, since the film is not yet continuous. Indeed, the error in estimating the thickness is higher when lower power is applied. For the very low power regime, the increase in pulse power leads to the drop of thickness and increased density during continuous film formation, as this correlation was reported by previous studies [34]. The thickness decrease (at this stage) with applying higher power was ascribed to the increase of nucleation density, as a consequence of combined deposition rate and energetic ions effect [35]. When increasing the power up to 750 W the density approaches the bulk density and the evaluated thickness is around 4.3 nm. Even if not fully continuous yet, this thickness can affect the transparency of the samples, as it was seen from the transmittance spectra (Figure 2). It should be noted that the electrical properties of those Cu thin film could not be measured, because they are not continuous.



(**a**) (**b**)

Figure 3. XRR spectra of Cu thin films deposited at 4 power settings of HIPIMS (scattering), and the fitting of the spectra (full line) (**a**); along with the resulted density and thickness variation as a function cathode power fed (**b**).

The Ag thin film were obtained by using DC magnetron sputtering, and the power interval was set from 100 to 250 W. The peak of transmittance does not exceed 80% in any of the cases, this being the maximum transmission in the visible range (Figure 4). The reflectivity in the IR spectra increases with increasing power, due to the increase of the thickness. The samples obtained at 200 and 250 W, respectively, have relatively high reflectivity, specific to the metallic layers. The absorption spectra on the other hand shows a maximum for the 150 W sample, due to the nanostructured nature of the thin film. This aspect suggests that silver films are continuous in the selected power interval.



(**a**) (**b**) (**c**)

Figure 4. Spectrophotometric curves, (**a**) reflectivity, (**b**) transmittance and (**c**) absorbance of Ag thin films deposited at different DC powers, from 100 to 250 W.

The surface morphology of the samples was investigated using electron microscopy, typical images being represented in Figure 5. The images confirm the fact that there is a nanostructured nature of the surface, with smoother and more continuous surface for the samples obtained at higher power inputs, 200 and 250 W, respectively. The sample obtained at 150 W has the most pronounced texturing of the surface, in agreement with the higher absorption previously observed. The sample obtained at 100 W of power input is also textured, with apparent holes on the surface.

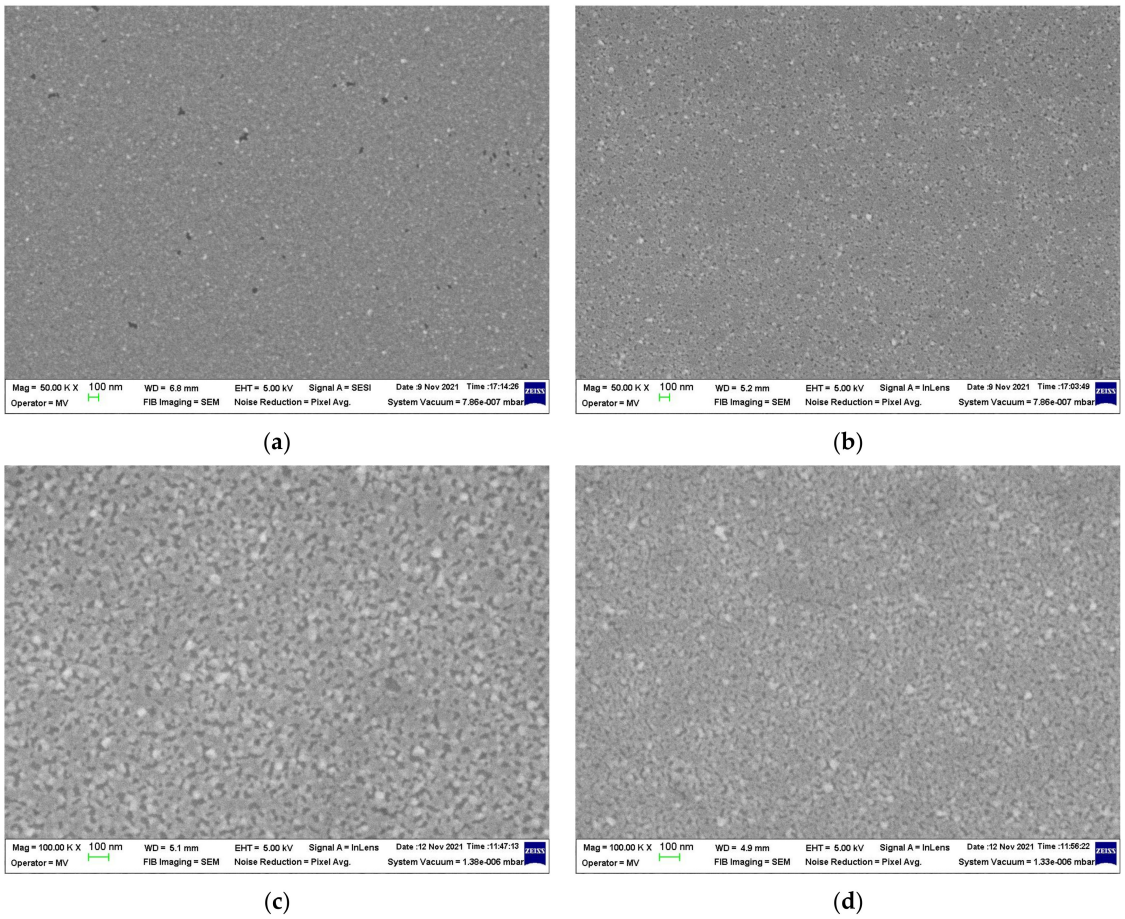


Figure 5. SEM images of the Ag samples obtained at different DC power inputs: (**a**) AgDC250, (**b**) AgDC200, (**c**) AgDC150, and (**d**) AgDC100.

The variation of electrical resistivity as a function of measured thickness is represented in Figure 6. The resistivity of the films changes abruptly in a very narrow thickens interval, corresponding to the increase of DC power from 100 to 150 W. This is a clear indication that, for these conditions, the layer is at the edge of coalescence. The resistivity remains almost constant, between 2.5 and 3.5 ($\Omega \times$ cm) $\times 10^{-5}$, once a certain thickness is attained, around 8.5 nm.

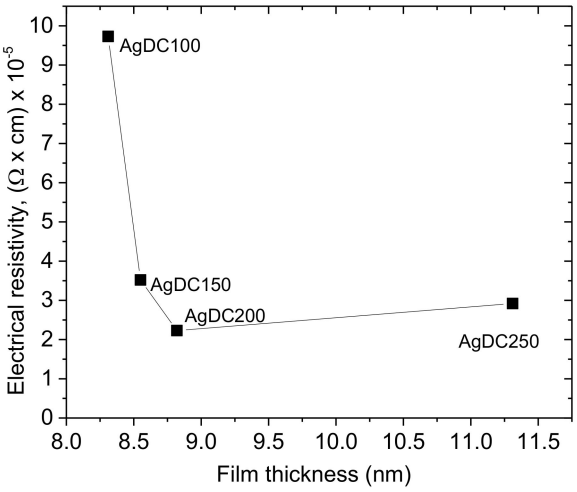
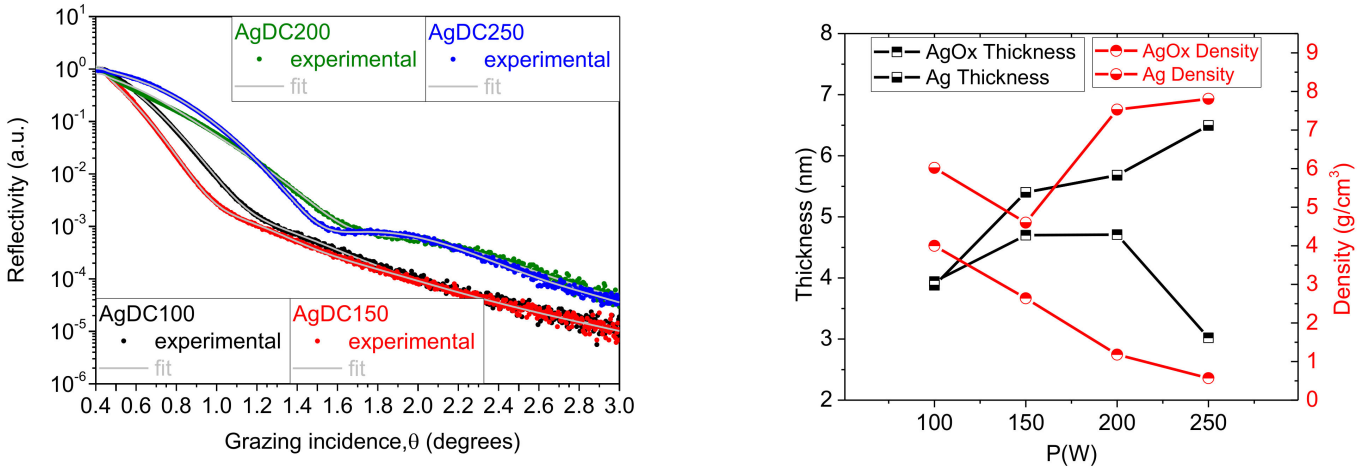


Figure 6. Average resistivity of the Ag thin films obtained at different HiPIMS powers, as a function of measured film thickness.

The XRR spectra of Ag thin films as a function of the applied power are presented in Figure 7, along with the results of density and thickness. Even though the specimens were exposed to the ambient atmosphere and an Ag-based oxide is present, the increase in thickness of Ag thin film with the applied power confirms the results previously obtained. As in the case of CuHIP monolayer, the XRR spectra of the thicker AgDC layer presents more visible interference induced oscillations. The formed Ag oxide exhibited a density decrease with applied power in benefit of Ag layer, except for AgDC150. It is to be noted that the different behavior of the AgDC150 sample was also observed from the optical characteristics, where a maximum of the absorption spectra for the mentioned layer was registered from the SEM images, where pronounced texturing was observed. This confirms the nanostructured nature of the sample obtained at these experimental conditions.

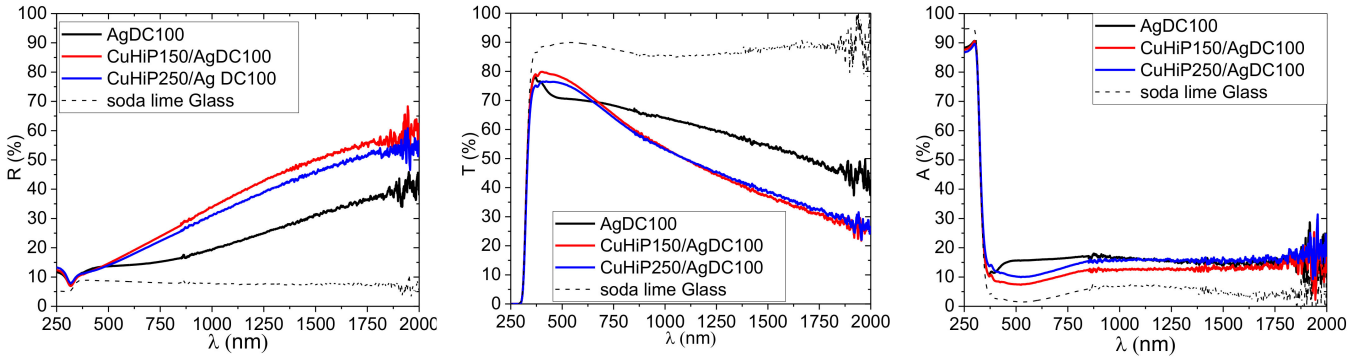


(**a**) (**b**)

Figure 7. XRR spectra of Ag thin films deposited at 4 power settings of DC (scattering), and the fitting of the spectra (full line) (**a**); along with the resulted density and thickness variation as a function cathode power fed (the error bars are within symbol limit) (**b**).

3.2. Cu/Ag Bilayers

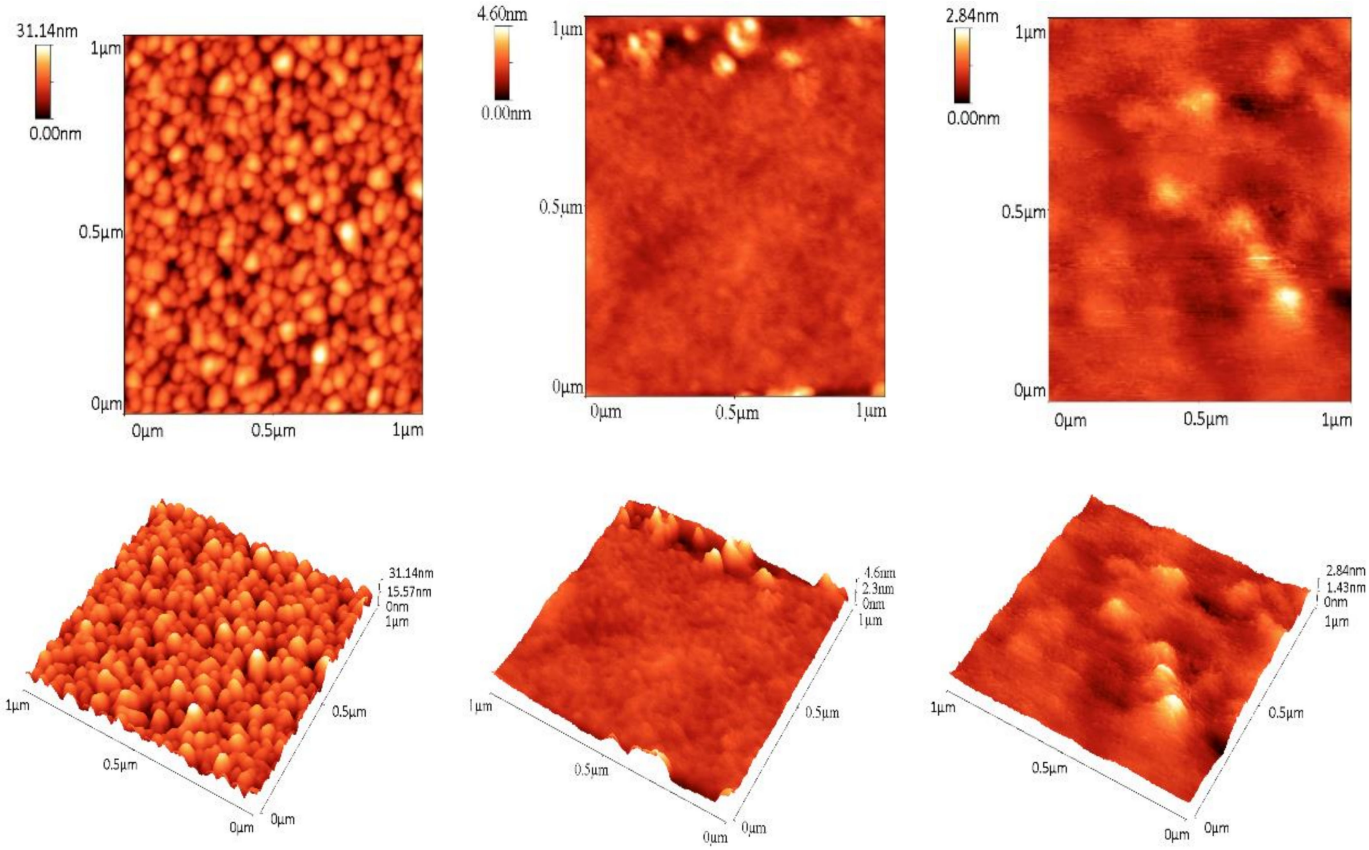
From the individual characterization of the Cu and Ag monolayers, it resulted that the most promising process conditions to obtain Cu discontinuous layers are obtained for a HiPIMS power input of 150 and 250 W, respectively. On the other hand, the silver layer obtained at 100 W of DC power is continuous, has the highest transmission in the visible range, but has a very poor conductivity. By adding a Cu seed layer before the deposition of Ag the quality of the obtained structure in terms of optical and electrical characteristics can be improved. The spectrophotometric curves are presented in Figure 8 for the bilayers of Cu at 150 and 250 W, respectively, and Ag at 100 W. For comparison, the corresponding curves for Soda Lime Glass and Ag at 100 W DC power deposited on glass are also presented. The Cu addition leads to a significant increase of reflectivity in the IR domain, with very small differences between the two versions. This finding is in line with the results obtained in Ref. [7] in the sense that once a certain minimum quantity of Cu is added, further addition of Cu does not add beneficial effect on the coalescence of silver layer. The transmittance of this structure is kept at ~80% within the visible range, making it suitable for application where good optical transparency is required. One interesting feature is that the absorbance is also decreasing, suggesting that the nanostructured nature of the Ag film is changed by the addition of the Cu seed layer.



(**a**) (**b**) (**c**)

Figure 8. Reflectivity (**a**), transmission (**b**) and absorption (**c**) spectra of Ag DC100 monolayer compared with the bilayers including Cu HiP150 and CuHiP250.

Indeed, the AFM images depicted in Figure 9 show that the Ag layer deposited directly on the silicon substrate has a relatively high roughness, Ra = 3.81 nm, whereas the samples that contain Cu seed layer are much smoother with roughness Ra = 0.237 nm for Cu150Ag100 samples and Ra = 0.224 nm for the Cu250Ag100 samples, one order of magnitude smaller than the Ag layer.



(**a**) (**b**) (**c**)

Figure 9. AFM images of Ag DC 100 monolayer (**a**) compared with the bilayers Cu150 Ag100 (**b**) and Cu250 Ag100 (**c**).

The resistivity of the thin film is also significantly decreased by the addition of Cu as a seed layer, due to the better wetting of the substrate and formation of a continuous layer. The variation of the Ag100 layer resistivity, with and without the Cu seeding, is represented in Figure 10. It is to be noted that the resistivity is significantly decreased when adding the Cu seeding layer, from 9.73 × 10^{-5} (Ω × cm) to 2.23 × 10^{-5} (Ω × cm), whereas the addition of different amounts of Cu does not lead to significant changes. The values for the resistivity are comparable with the ones obtained at higher power inputs on the Ag target, corresponding to the thicker Ag layer.

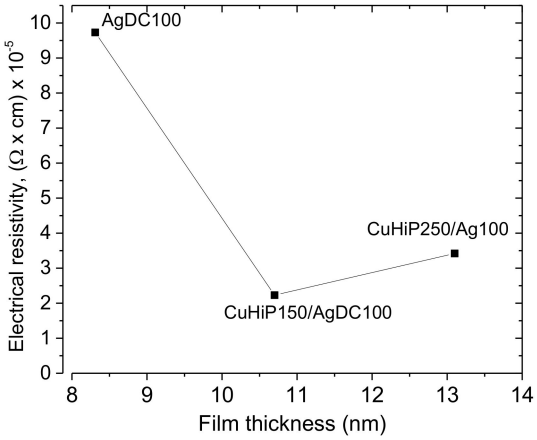
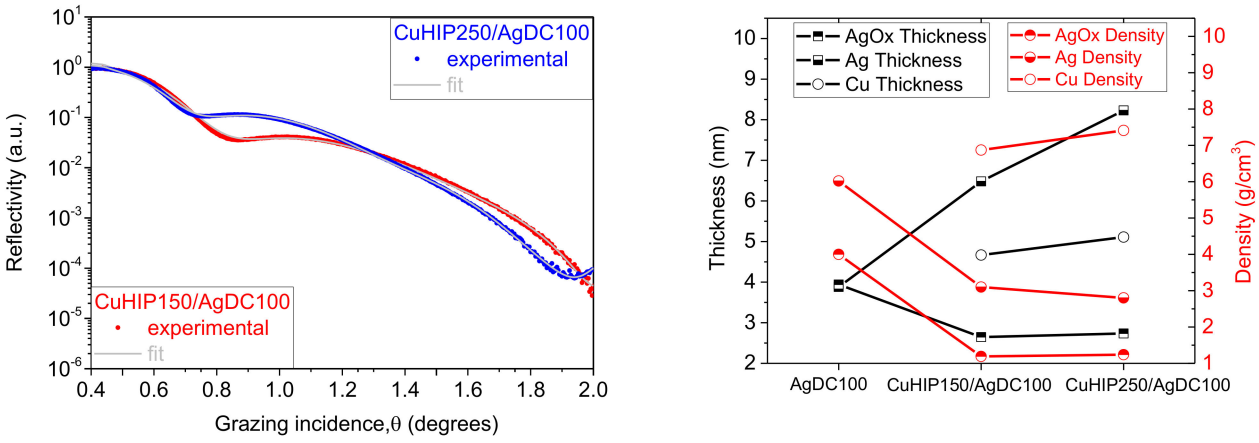


Figure 10. Average resistivity of the Ag100 layer as a function of Cu content.

Figure 11a shows the XRR spectra of Cu/Ag bilayers as a function of the HIPIMS power applied. The resulting thickness and densities are represented in Figure 11b, along with the thickness and densities resulted for the AgDC100 layer for comparison. In the case of Cu seed layer, note the small increasing tendency of thickness (up to 5 nm) and density (up to ~7 g/cm^3) at 250 W. Similar behavior was observed also for Ag thickness, slightly higher values being obtained when increasing the power input. However, adding more Cu did not lead to a significant improvement in the overall density of Cu/Ag bilayers. What it is interesting to note is the relative proportion of the oxide as compared with the unoxidized Ag layer. Indeed, for the AgDC100 layer, the thickness of the two components is equal around 4 nm. When adding the Cu seed layer, the thickness of the oxide decreases and that of Ag increases, showing a better stability to oxidation.



(**a**) (**b**)

Figure 11. XRR spectra of Cu/Ag bilayers (scattering), and the fitting of the spectra (full line) (**a**); along with the resulted density and thickness variation as a function of Cu content (the error bars are within symbol limit) (**b**).

4. Conclusions

The effect of Cu addition as a seed layer for continuous, transparent conductive Ag coatings was investigated in an industrial scale setup. The fine tuning of the thickness needed for this purpose was achieved by using a very short process where the substrates passed in front of the target only one time, for a short period of less than 10 s. Additional control over the deposition rate of Copper was obtained by tuning the repetition frequency of the high power pulses, and keeping the pulse characteristics constant. The Cu addition is proven to reduce significantly the resistivity of the film, while maintaining a high transparency in the visible domain. This is done by improving the wetting properties of growing film and reducing the coalescence thickness. The resulting layer is significantly smoother, with surface roughness 10 times smaller than the one of Ag alone.

5. Patents

Patent application OSIM: Sobetkii A., Visan M., Capatina V., Iordache I., Banciu C.A., Vitelaru C., Parau A.C., Pana I., Technology for controlling the coalescence of conductive transparent coatings made of silver with copper addition, A/00768, 9 December 2021.

Author Contributions: Conceptualization, C.V., A.S. and I.I.; methodology, C.V., A.S. and I.I.; formal analysis, M.D.; investigation, A.C.P., M.D., I.P. and L.R.C.; data curation, A.C.P. and L.R.C.; writing—original draft preparation, C.V., L.R.C. and I.P.; writing—review and editing, A.S. and I.I.; supervision, C.V.; validation, I.P.; project administration, C.V., A.S. and I.I. All authors have read and agreed to the published version of the manuscript.

Funding: This work was supported by a grant of the Romanian Ministry of Education and Research, CCDI-UEFISCDI Project number PN-III-P2-2.1-PTE-2019-0763, contract no7PTE/2020, within PNCDI.

Data Availability Statement: Not applicable.

Acknowledgments: We acknowledge the support of the Ministry of Research, Innovation and Digitization, CNCS/CCCDI–UEFISCDI, through the Core Program, Project no. 18N/2019 and through Program 1—Development of the national research-development system, Subprogram 1.2—Institutional performance-Projects to finance the excellent RDI, Contract no. 18PFE/30.12.2021.

Conflicts of Interest: The authors declare no conflict of interest. The funders had no role in the design of the study; in the collection, analyses, or interpretation of data; in the writing of the manuscript, or in the decision to publish the results.

References

1. Gong, C.; Huang, C.; Miller, J.; Cheng, L.; Hao, Y.; Cobden, D.; Kim, J.; Ruoff, R.S.; Wallace, R.M.; Cho, K.; et al. Metal Contacts on Physical Vapor Deposited Monolayer MoS2. *ACS Nano* **2013**, *7*, 11350–11357. [CrossRef] [PubMed]
2. Lee, I.; Lee, J.-L. Transparent Electrode of Nanoscale Metal Film for Optoelectronic Devices. *J. Photonics Energy* **2015**, *5*, 057609. [CrossRef]
3. Zhao, G.; Kim, S.M.; Lee, S.G.; Bae, T.S.; Mun, C.W.; Lee, S.; Yu, H.; Lee, G.H.; Lee, H.S.; Song, M.; et al. Bendable Solar Cells from Stable, Flexible, and Transparent Conducting Electrodes Fabricated Using a Nitrogen-Doped Ultrathin Copper Film. *Adv. Funct. Mater.* **2016**, *26*, 4180–4191. [CrossRef]
4. Zhao, G.; Shen, W.; Jeong, E.; Lee, S.G.; Chung, H.S.; Bae, T.S.; Bae, J.S.; Lee, G.H.; Tang, J.; Yun, J. Nitrogen-Mediated Growth of Silver Nanocrystals to Form UltraThin, High-Purity Silver-Film Electrodes with Broad Band Transparency for Solar Cells. *ACS Appl. Mater. Interfaces* **2018**, *10*, 40901–40910. [CrossRef]
5. Wang, W.; Song, M.; Bae, T.S.; Park, Y.H.; Kang, Y.C.; Lee, S.G.; Kim, S.Y.; Kim, D.H.; Lee, S.; Min, G.; et al. Transparent Ultrathin Oxygen-Doped Silver Electrodes for Flexible Organic Solar Cells. *Adv. Funct. Mater.* **2014**, *24*, 1551–1561. [CrossRef]
6. Erdogan, N.; Erden, F.; Astarlioglu, A.T.; Ozdemir, M.; Ozbay, S.; Aygun, G.; Ozyuzer, L. ITO/Au/ITO Multilayer Thin Films on Transparent Polycarbonate with Enhanced EMI Shielding Properties. *Curr. Appl. Phys.* **2020**, *20*, 489–497. [CrossRef]
7. Jamnig, A.; Pliatsikas, N.; Abadias, G.; Sarakinos, K. On the Effect of Copper as Wetting Agent during Growth of Thin Silver Films on Silicon Dioxide Substrates. *Appl. Surf. Sci.* **2021**, *538*, 148056. [CrossRef]
8. Sarakinos, K. A Review on Morphological Evolution of Thin Metal Films on Weakly-Interacting Substrates. *Thin Solid Films* **2019**, *688*, 137312. [CrossRef]
9. Zhang, C.; Ji, C.; Park, Y.B.; Guo, L.J. Thin-Metal-Film-Based Transparent Conductors: Material Preparation, Optical Design, and Device Applications. *Adv. Opt. Mater.* **2021**, *9*, 2001298. [CrossRef]

10. Dalapati, G.K.; Kushwaha, A.K.; Sharma, M.; Suresh, V.; Shannigrahi, S.; Zhuk, S.; Masudy-Panah, S. Transparent Heat Regulating (THR) Materials and Coatings for Energy Saving Window Applications: Impact of Materials Design, Micro-Structural, and Interface Quality on the THR Performance. *Prog. Mater. Sci.* **2018**, *95*, 42–131. [CrossRef]
11. Stoessel, C.H. *Optical Coatings for Automotive and Building Applications*; Elsevier Ltd.: Amsterdam, The Netherlands, 2013; ISBN 9780857095947.
12. Ebner, D.; Bauch, M.; Dimopoulos, T. High Performance and Low Cost Transparent Electrodes Based on Ultrathin Cu Layer. *Opt. Express* **2017**, *25*, A240–A252. [CrossRef]
13. Yun, J. Ultrathin Metal Films for Transparent Electrodes of Flexible Optoelectronic Devices. *Adv. Funct. Mater.* **2017**, *27*, 1606641. [CrossRef]
14. Pliatsikas, N.; Jamnig, A.; Konpan, M.; Delimitis, A.; Abadias, G.; Sarakinos, K. Manipulation of Thin Silver Film Growth on Weakly Interacting Silicon Dioxide Substrates Using Oxygen as a Surfactant. *J. Vac. Sci. Technol. A* **2020**, *38*, 043406. [CrossRef]
15. Jamnig, A.; Pliatsikas, N.; Konpan, M.; Lu, J.; Kehagias, T.; Kotanidis, A.N.; Kalfagiannis, N.; Bellas, D.V.; Lidorikis, E.; Kovac, J.; et al. 3D-to-2D Morphology Manipulation of Sputter-Deposited Nanoscale Silver Films on Weakly Interacting Substrates via Selective Nitrogen Deployment for Multifunctional Metal Contacts. *ACS Appl. Nano Mater.* **2020**, *3*, 4728–4738. [CrossRef]
16. Riveiro, J.M.; Normile, P.S.; Andrés, J.P.; González, J.A.; De Toro, J.A.; Muñoz, T.; Muñiz, P. Oxygen-Assisted Control of Surface Morphology in Nonepitaxial Sputter Growth of Ag. *Appl. Phys. Lett.* **2006**, *89*, 201902. [CrossRef]
17. Anders, A.; Byon, E.; Kim, D.H.; Fukuda, K.; Lim, S.H.N. Smoothing of Ultrathin Silver Films by Transition Metal Seeding. *Solid State Commun.* **2006**, *140*, 225–229. [CrossRef]
18. Gu, D.; Zhang, C.; Wu, Y.K.; Guo, L.J. Ultrasmooth and Thermally Stable Silver-Based Thin Films with Subnanometer Roughness by Aluminum Doping. *ACS Nano* **2014**, *8*, 10343–10351. [CrossRef]
19. Fukuda, K.; Lim, S.H.N.; Anders, A. Coalescence of Magnetron-Sputtered Silver Islands Affected by Transition Metal Seeding (Ni, Cr, Nb, Zr, Mo, W, Ta) and Other Parameters. *Thin Solid Films* **2008**, *516*, 4546–4552. [CrossRef]
20. Jamnig, A.; Sangiovanni, D.G.; Abadias, G.; Sarakinos, K. Atomic-Scale Diffusion Rates during Growth of Thin Metal Films on Weakly-Interacting Substrates. *Sci. Rep.* **2019**, *9*, 6640. [CrossRef]
21. Elofsson, V.; Almyras, G.A.; Lü, B.; Garbrecht, M.; Boyd, R.D.; Sarakinos, K. Structure Formation in Ag-X (X = Au, Cu) Alloys Synthesized Far-from-Equilibrium. *J. Appl. Phys.* **2018**, *123*, 165301. [CrossRef]
22. Misják, F.; Barna, P.B.; Radnóczi, G. Growth of Nanocomposite in Eutectic Cu-Ag Films. *Thin Solid Films* **2010**, *518*, 4247–4251. [CrossRef]
23. Lundin, D.; Hecimovic, A.; Minea, T.; Anders, A.; Brenning, N.; Gudmundsson, J.T. Physics of High Power Impulse Magnetron Sputtering Discharges. In *High Power Impulse Magnetron Sputtering: Fundamentals, Technologies, Challenges and Applications*; Elsevier: Amsterdam, The Netherlands, 2019; pp. 265–332, ISBN 9780128124543.
24. Greczynski, G.; Lu, J.; Jensen, J.; Bolz, S.; Kölker, W.; Schiffers, C.; Lemmer, O.; Greene, J.E.; Hultman, L. A Review of Metal-Ion-Flux-Controlled Growth of Metastable TiAlN by HIPIMS/DCMS Co-Sputtering. *Surf. Coatings Technol.* **2014**, *257*, 15–25. [CrossRef]
25. Pana, I.; Parau, A.C.; Dinu, M.; Kiss, A.E.; Constantin, L.R.; Vitelaru, C. Optical Properties and Stability of Copper Thin Films for Transparent Thermal Heat Reflectors. *Metals* **2022**, *12*, 262. [CrossRef]
26. *SEMI Standard MF84-0312*; Test Method for Measuring Resistivity of Silicon Wafers with an In-Line Four-Point Probe. ASTM International: West Conshohocken, PA, USA, 2012.
27. Bolesta, I.; Velgosh, S.; Datsiuk, Y.; Karbovnyk, I.; Lesivtsiv, V.; Kulay, T.; Popov, A.I.; Bellucci, S.; Cestelli Guidi, M.; Marcelli, A.; et al. Optical, Infrared and Electron-Microscopy Studies of (Cdi)n Metallic Clusters in Layered CdI2 Crystals. *Radiat. Meas.* **2007**, *42*, 851–854. [CrossRef]
28. Ţălu, Ş.; Yadav, R.P.; Mittal, A.K.; Achour, A.; Luna, C.; Mardani, M.; Solaymani, S.; Arman, A.; Hafezi, F.; Ahmadpourian, A.; et al. Application of Mie Theory and Fractal Models to Determine the Optical and Surface Roughness of Ag–Cu Thin Films. *Opt. Quantum Electron.* **2017**, *49*, 256. [CrossRef]
29. Seal, K.; Nelson, M.A.; Ying, Z.C.; Genov, D.A.; Sarychev, A.K.; Shalaev, V.M. Growth, Morphology, and Optical and Electrical Properties of Semicontinuous Metallic Films. *Phys. Rev. B Condens. Matter Mater. Phys.* **2003**, *67*, 035318. [CrossRef]
30. Buttard, D.; Dolino, G.; Bellet, D.; Baumbach, T.; Rieutord, F. X-Ray Reflectivity Investigation of Thin p-Type Porous Silicon Layers. *Solid State Commun.* **1998**, *109*, 1–5. [CrossRef]
31. Braga, A.; Baratto, C.; Colombi, P.; Bontempi, E.; Salvinelli, G.; Drera, G.; Sangaletti, L. An Ultrathin TiO_2 Blocking Layer on Cd Stannate as Highly Efficient Front Contact for Dye-Sensitized Solar Cells. *Phys. Chem. Chem. Phys.* **2013**, *15*, 1–8. [CrossRef]
32. Sarakinos, K.; Magnfält, D.; Elofsson, V.; Lü, B. Atomistic View on Thin Film Nucleation and Growth by Using Highly Ionized and Pulsed Vapour Fluxes. *Surf. Coatings Technol.* **2014**, *257*, 326–332. [CrossRef]
33. Sheldon, B.W.; Lau, K.H.A.; Rajamani, A. Intrinsic Stress, Island Coalescence, and Surface Roughness during the Growth of Polycrystalline Films. *J. Appl. Phys.* **2001**, *90*, 5097–5103. [CrossRef]
34. Warrender, J.M.; Aziz, M.J. Evolution of Ag Nanocrystal Films Grown by Pulsed Laser Deposition. *Appl. Phys. A* **2004**, *79*, 713–716. [CrossRef]
35. Warrender, J.M.; Aziz, M.J. Effect of Deposition Rate on Morphology Evolution of Metal-on-Insulator Films Grown by Pulsed Laser Deposition. *Phys. Rev. B Condens. Matter Mater. Phys.* **2007**, *76*, 045414. [CrossRef]